Recently Amplified Interannual Variability of Great Lakes ice cover and its Connection to Sea Ice over the Bering and Chukchi Seas

Yuchun Lin[1], Ayumi Fujisaki-Manome[2], and Jia Wang[3]

[1]Cooperative Institute for Great Lakes Research
[2]University of Michigan-Ann Arbor
[3]National Oceanic and Atmospheric Administration (NOAA)

November 24, 2022

Abstract

The interannual variability of the annual maximum ice cover (AMIC) of the Great Lakes is generally dominated by a dipole pattern over mid-latitude North America and Western Alaska via a ridge-trough system. We discovered a significant breakpoint in the winter of 1997/98 after which AMIC increased its interannual variability and negatively correlated with sea ice coverage over the Bering and Chukchi Seas in the preceding Novermber and Decemeber. The first covarying mode of the 500hPa geopotential height and surface air temperature indicated that the dipole pattern shifted northward to the northern Rocky Mountains after the breakpoint. Correlati The correlations with AMIC of the other well-known teleconnection patterns such as the El Niño–Southern Oscillation on AMIC became insignificant after the brekpoint and were replaced by that from the Eastern Pacific Oscillaiton, which likely controlled the interannual variabilities of AMIC and sea ice cover the Bering and Chukchi Seas.

Recently Amplified Interannual Variability of Great Lakes ice cover and its Connection to Sea Ice over the Bering and Chukchi Seas

Y.C. Lin[1], A. Fujisaki-Manome[1,2], and J. Wang[3]

[1] Cooperative Institute for Great Lakes Research, University of Michigan, Ann Arbor, Michigan.

[2] Climate&Space Sciences and Engineering, University of Michigan, Ann Arbor, Michigan

[3] Great Lakes Environmental Research Laboratory, NOAA, Ann Arbor, Michigan

Corresponding author: Yuchun Lin (yuchlin@umich.edu)

†Additional author notes should be indicated with symbols (current addresses, for example).

Key Points:

- A significant increased interannual variability of the Great Lakes ice cover is found to connect with the upstream sea ice concentration.
- Analyses suggested that the variability of ice cover is dominated by surface air tempearture driven by geopotential hight at 500hPa.
- Influence on the ice cover has changed from multiple well-known teleconnection patterns to a single pattern dominating the Gulf of Alaska.

Abstract

The interannual variability of the annual maximum ice cover (AMIC) of the Great Lakes is generally dominated by a dipole pattern over mid-latitude North America and Western Alaska via a ridge-trough system. We discovered a significant breakpoint in the winter of 1997/98 after which AMIC increased its interannual variability and negatively correlated with sea ice coverage over the Bering and Chukchi Seas in the preceding Novermber and Decemeber. The first covarying mode of the 500hPa geopotential height and surface air temperature indicated that the dipole pattern shifted northward to the northern Rocky Mountains after the breakpoint. Correlati The correlations with AMIC of the other well-known teleconnection patterns such as the El Niño–Southern Oscillation on AMIC became insignificant after the brekpoint and were replaced by that from the Eastern Pacific Oscillaiton, which likely controlled the interannual variabilities of AMIC and sea ice cover the Bering and Chukchi Seas.

Plain Language Summary

The annual maximum ice cover (AMIC) of the Great Lakes is generally impacted by a pair of air pressure differences from the long-term averages over the mid-latitude North America and Western Alaska. In this study, we discovered that AMIC's year-to-year fluctuations significantly increased after the winter of 1997/98 and the fluctuations started to show an opposite behabior aginst the fluctuations of sea ice over the Bering and Chukchi Seas in the earlier winter season. The analyses on atmospheric circulation and surface air temperature indicated that the pair of air pressure differences moved norward to the northern Rocky Mountains after the breakpoint. As a result, the well-known teleconnection patterns such as El Niño–Southern Oscillation started not to correlate with AMIC after the breakpoint. Instead, the Eastern Pacific Oscillaiton explained the year-to-year fluctuations of AMIC and sea ice cover over the Bering and Chukchi Seas.

1 Introduction

An emerging challenge in climate sciences is to understand how the changes in the Arctic region influence mid-latitude atmospheric patterns and consequently local extreme weather. The Arctic Ocean has warmed significantly and the Arctic sea ice has declined rapidly over the past two decades in responses to global warming [Serreze & Francis, 2006; Gillett et al., 2008; Carmack & Melling, 2011], which is known as Arctic Amplification [Cohen et al., 2014]. Recent studies suggested that loss of summer sea ice over the marginal oceans in the Arctic triggered changes in planetary waves, resulting in extreme weather over Eurasia [Honda, et al., 2009; Cohen et al., 2014; Ogi et al., 2015] and North America [Chan et al., 2009; Cohen et al., 2014, 2018; Overland and Wang, 2018].

The North American Great Lakes (hereafter, the Great Lakes), accounting for one fifth of the world's freshwater, are partially frozen each year with high year-to-year fluctuations of annual maximum ice cover (AMIC). Extremely cold winters with high AMICs have huge impacts to the surrounding population [Assel et al., 1996, 2000], the economy [Niimi, 1992], and the environment and ecosystems [Vanderploeg et al., 1992; John et al., 1995]. Studies have shown that the ice cover has decreased in recent decades in responses to global warming [Magnuson., 2000; Titze & Austin, 2014]. These decreasing trends are observed in all five lakes since the 1980s [Wang et al., 2012] .

The AMIC has presented high year-to-year fluctuations from 1980 to 2017, with the lowest of 12% in 2002 and the highest of 93% (Fig. 1a). The winter severity and associated AMIC were mostly in response to the combinations of regional and northern hemisphere climates. A number of studies investigated the relation between AMIC and teleconnection patterns that involve North America such as the El Niño and Southern Oscillation (ENSO) [Bamston et al., 1997], the Pacific-North American Teleconnection Pattern (PNA) [Wallace and Gutzler, 1981], the Tropical-North Hemisphere Pattern (TNH) [Mo and Livezey, 1986], the North Atlantic Oscillation (NAO) [Hurrell, 1995] or the Arctic Oscillation (AO) [Thompson & Wallace, 1998] in the past decades [Smith, 1991; Hanson et al., 1992; Assel, 1998; Assel & Robertson, 1995; Rodionov & Assel, 2000, 2001; Assel et al., 2003; Wang et al., 2010, 2012, 2018]. Almost half of the low AMIC were suggested to be associated with strong positive ENSO events [Assel, 1998, Assel & Rodionov, 1998] and had high positive correlations with PNA and THN [Assel, 1992; Assel & Rodionov, 1998]. The NAO/AO was found to partially contribute to ice cover in some areas of Great Lakes [Assel et al., 1985; Assel et al., 2000; Rodionov & Assel., 2001]. Recent studies also showed that individual AMIC could be affected linearly to NAO and non-linearly to ENSO at the same time [Bai et al., 2012], which complicates the diagnosis of the weather patterns related to Great Lakes ice cover. These collectively suggest that a single climate index is unable to explain the atmospheric circulations that control the winter severity over the Great Lakes and AMIC, and that a key mechanism that sets up such atmospheric circulations needs to be identified.

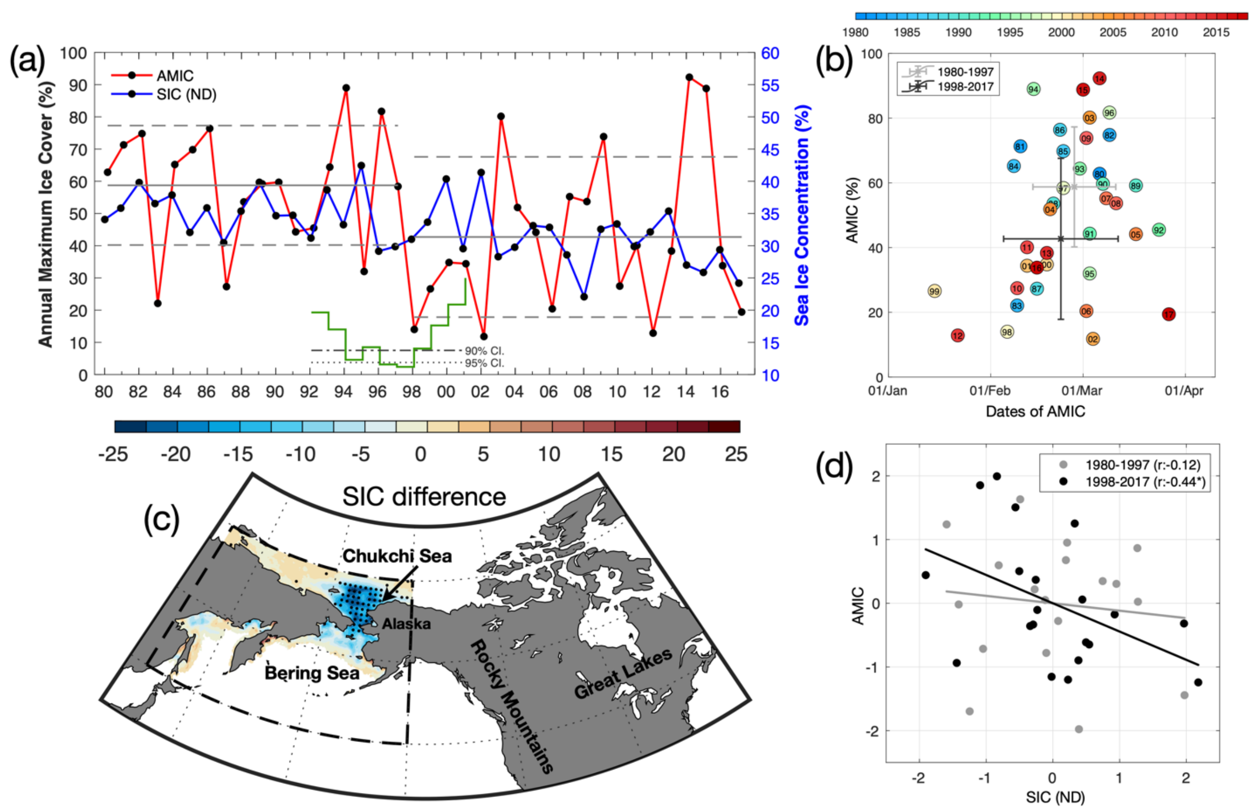

Figure 1. (a) Annual maximum ice cover (AMIC, %) from 1980 to 2017 (red line with black dots). Blue line with black dots indicates the sea ice concentration (SIC) averaged within November-December over Bering Seas (black-dashed box in Fig.1c). Black solid lines and gray

dashed lines indicate the means and standard deviations of AMIC in earlier (1980-1997) and later (1998-2017) periods. Green line indicates the t-test p-value of the separation year for periods before and after. Dotted and dotted-dashed lines indicate the 95% and 90% confidence level, respectively. (b) Scatter plot of dates of AMIC versus AMIC from 1980 to 2017. Crosses indicate the mean and error bars are the standard deviation for dates of AMIC (horizontal) and AMIC (vertical) of earlier (gray) and later (black) periods. (c) Sea ice concentration difference between the two periods (later minus earlier period). Dots indicate that the difference between the two periods reaches the 95% confidence interval based on t-test. Black-dashed box indicates the region for the blue line in Fig. 1a. (d) Scatter plot of the normalized sea ice concentration and AMIC (shown in Fig. 1a) for the earlier period (black) and later period (red).

How can these opposite behaviors of ice cover in the far-off locations be explained? We addressed this question by revisiting the atmospheric patterns related to AMIC in the periods before and after the breakpoint in the winter of 1997/98 (Fig. 1a). Statistical and composite analyses were conducted using the National Centers for Environmental Prediction (NCEP) dataset, sea ice data in the Bering and Chukchi Seas, and the Great Lakes ice cover dataset.

2 Data and Methods

We applied a series of Student’s t-tests to AMIC obtained from the National Oceanic and Atmospheric Administration/Great Lakes Environmental Research Laboratory (NOAA/GLERL) ice atlas databse [Wang et al., 2017; Yang et al., 2020] to identify a statistically significant breakpoint after which a standard deviation (a proxy of year-to-year fluctuations) increased (Fig.1a). We evaluated the relation of AMIC and sea ice coverage over the Bering and Chukchi Seas with atmospheric conditions represented by 500 hPa geopotential height and surface air temperature. Monthly gridded Arctic sea ice concentration was obtained from the National Snow and Ice Data Center (NSIDC) dataset, which traces back to 1850 and has spatial resolution of ¼° x ¼° covering from 30°N to the North Pole [Walsh et al., 2016]. Monthly atmospheric data were obtained from the National Centers for Environmental Prediction/Department of Energy Atmospheric Model Intercomparison Project II (known as NCEP reanalysis II) [Kanamitsu et al., 2002] from January 1979 to June 2017. The reanalysis data has 2.5° spatial resolution in both longitude and latitude and the domain for this study is between 10°N-90°N and 60°W-210°W. The NCEP geopotential height and atmospheric temperature are located at 17 pressure levels. Geopotential height at 500 hPa (Φ500) and air temperature at 2 m (T_{2m}), which has high connection to the AMIC variation [Rodionov & Assel, 2003], was used.

The monthly climate indices of ENSO [Bamston et al., 1997], PDO [Mantua et al., 1997], NAO [Hurrell, 1995], AO [Thompson and Wallace, 1998], and PNA [Barnston and Livezey, 1987] that highly influences the weather of the northern hemisphere were selected to examine the connections with AMIC. Daily Eastern Pacific Oscillation (EPO) [Barnston and Livezey, 1987], a relatively new climate index, was also used after calculating monthly averages to explain the amplification of AMIC. The EPO index is defined based on the difference of Φ500 where the region of (55°N-65°N, 125°W-160°W) is subtracted from (20°N-35°N, 125°W-160°W) obtained from NOAA/Earth System Research Laboratory (https://psl.noaa.gov/data/timeseries/daily/EPO/). These climate indices are obtained from the NOAA Climate Prediction Center (CPC) and ESRL/PSL GEFS reforecast 2 ensemble forecasts.

The empirical orthogonal function (EOF) and the singular value decomposition (SVD) were applied to monthly and winter (December-February) values to understand the main weather patterns related to AMIC and SIC_{ND}. In order to understand the major weather patterns related to the AMIC in the three periods, SVD analyses were applied to the 2m air temperature (T_{2m}) and geopotential height at 500 hPa (Φ500), averaged from December to the following February for the entire period (1980-2017), the earlier period (1980-1997), and the later period (1998-2017) . These periods were chosen based on the most significant separation year 1997/98 breakpoint (Fig. 1a). The domain of T_{2m} is focused on North America and the region of geopotential height is chosen to cover the North Pacific and North America. The 95% significance level was used to determine if the calculated correlation coefficients are statistically significant or not.

3 Results

3.1 Negative correlation of AMIC in the Great Lakes with sea ice coverage over the Bering-Chukchi Seas after 1997/98

AMIC in the Great Lakes presented high year-to-year fluctuations from 1980 to 2017 (Fig. 1a), with the standard deviation of 23%, the highest of 93% in 2013/14, and the lowest of 12% in 2011/12. There is a significantly decreasing trend of AMIC (-4.7%/decade) during this period.

There was a statistically significant breakpoint in the winter of 1997/98, identified with the lowest t-test p-value (green line in Fig. 1a), which coincided with one of the largest ENSO events (Fig. 1a) of the 20th century. After this breakpoint AMIC experienced large interannual fluctuations compared to the years before. It is worth noting that both the highest and lowest AMIC appeared after the breakpoint. The mean±standard deviation for AMIC is 59±18% and 43±25% before and after the breakpoint, respectively. Despite the several high AMICs in the later period, the mean has largely decreased from the earlier period and the long-term average suggested by the previous studies (55% in 1963-2010) [Bai et al., 2012; Wang et al., 2018]. The changes after the breakpoint are consistent with the previous study identified a step change decrease in AMIC or regime change in Lake Superior after this breakpoint [Van Cleave et al., 2014].

The timing of AMICs were primarily from late February to early March (Fig. 1b). The average date of AMIC was on February 24 and the standard deviation of the peak dates was 15 days. Increased interannual fluctuations represented by a standard deviation was also presented on the date of AMIC, which can be seen from the standard deviation crosses of the two periods in Fig. 1b. The standard deviation of the date of AMIC has increased significantly from 12 days in earlier period to 17 days in the later period, after the 1997/98 breakpoint.

Notably, after this breakpoint loss of sea ice concentration (SIC) over the Bering and Chukchi Seas in November-December (SIC_{ND}) accelerated twofold, from insignificant -1.7% per decade for the later period (1980-1997) to significant -3.7% for the earlier period (1998-2017) (Fig. 1a). The mean SIC_{ND} in the Bering and Chukchi Seas was also significantly lower in the 1998-2017 period than the 1980-1997 period, with maximum difference reaching 25% (Fig. 1c). Furthermore, during the earlier period the AMIC and SIC_{ND} started to present a significant negative correlation (r=-0.44), while after the breakpoint, there was no significant correlation between the two (Fig. 1d).

3.2 Dipole pattern in the covarying mode of 500 hPa geopotential height and surface air temperature

The SVD mode 1 from 1980 to 2017 accounts for 50% of the total variation (Fig. 2a) and it is well separated from the higher modes. The spatial pattern 1 (*sp1*) of T_{2m} shows a large negative pattern covering the region west of the Great Lakes and a positive pattern over Alaska, Mexico, and the Canadian Arctic Archipelago (CAA). The *sp1* of Φ500 shows a dipole structure, where the negative is located at central North America, corresponding to *sp1* of air temperature (color in Fig. 2a), and the positive is centered on the Bering Strait with extension towards Gulf of Mexico. The expansion coefficient 1 (*ec1*) of T_{2m} and Φ500 were highly correlated with each other ($r \sim 0.85$) and they also had significant correlation with AMIC (red line in Fig. 2d), where the $r \sim -0.7$ for T_{2m} and $r \sim -0.6$ for the Φ500. This SVD mode 1 indicates that the variation of AMIC in the past four decades was directly related to the T_{2m}, which was most related to a dipole Φ500 pattern over the northern Pacific and North America. During the high AMIC years, the positive anomaly of Φ500 over the Bering and Chukchi Seas and its negative over central North America (so-called 'the ridge-trough dipole pattern') steered the cold air mass from the Arctic across the Rocky Mountains into central North America [Bai and Wang, 2012]. This anomalous circulation is reversed during low AMIC years.

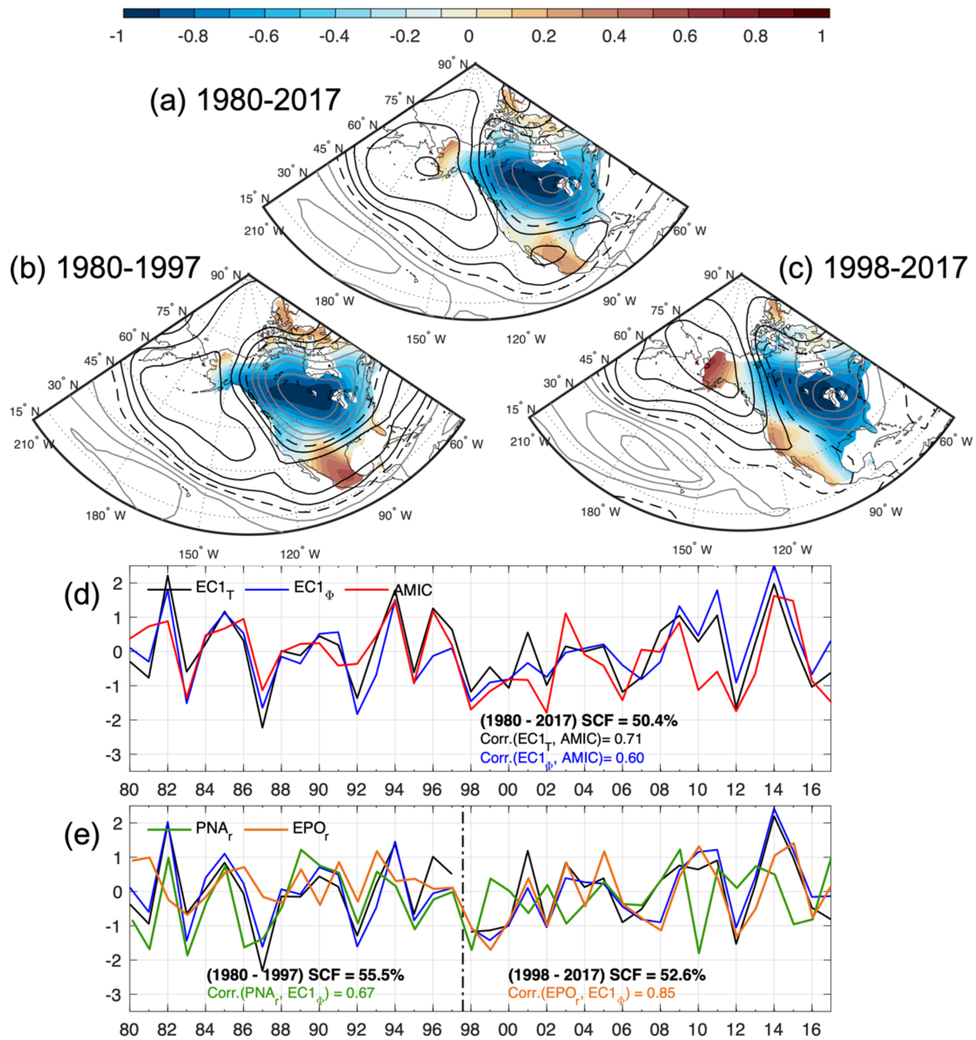

Figure 2. Spatial patterns of SVD modes 1 for T_{2m} (color) and Φ500 (contour) averaged over December to February of (a) 1980 to 2017, (b) 1980 to 1997, and (c) 1998 to 2017. Expansion coefficients of T_{2m} ($EC1_{T2m}$, black) and Φ500 ($EC1_{\Phi500}$, blue) of (d) 1980 to 2017, and (e) 1980 to 1997 (years before vertical dashed line) 1998 to 2017 (years after vertical dashed line). All expansion coefficients are normalized by their respective standard deviations. Vertical dashed line in (e) indicates the year of 1997 for separation. SCF is the square covariance fraction and r is the correlation coefficient between the two expansion coefficients. Red line in (d) is the AMIC, green line in (e) is the PNA_r, and orange line in (e) is the EPO_r, where the subscript "*r*" indicates the reversed index. Both AMIC and EPO are normalized by their standard deviations, except for PNA. Corr(*A*, *B*) denotes the correlation coefficient between *A* and *B*. All Corr(*A*, *B*) listed here reach the 95% confidence interval.

The SVD mode 1 on T_{2m} and Φ500 presented a notable change after the 1997/98 breakpoint. The mode 1 of the earlier (1980-1997) and the later (1998-2017) periods accounted for 55.5% and 52.6% of their total variances, respectively. The *sp1* of T_{2m} in both periods a have negative maximum west of the Great Lakes and the *sp1* of Φ500 have a dipole structure over the North Pacific and North America. In the earlier period, the *sp1* of T_{2m} presented a wider range of the negative maximum west of the Great Lakes (Fig. 2b) compared to the later period (Fig. 2c). Most notably, the dipole structure of the *sp1* of Φ500 shifted its center northeastward over the northern part of the Rocky Mountains (Fig. 2b,c) . The *ec1* of the earlier and the later periods captured the variations of AMIC in each period (Fig. 2e). The *ec1* of T_{2m} and Φ500 in both the earlier and later periods had significant correlations with AMIC, where the r ~ 0.71 and 0.71 (r ~ 0.77 and 0.65) for T_{2m} and Φ500 in the earlier period (later period).

This shift in the pattern of T_{2m}-Φ500 SVD mode 1 after the 1997/98 breakpoint also revealed the changes in contributions from climate indices. The *sp1* of Φ500 in the earlier period shows a reversed PNA-like pattern with positive values over the North Pacific and negative in North America (Fig. 2b). Both *ec1* of T_{2m} and Φ500 in the earlier period had a significant correlation coefficient r ~ 0.67 with the reversed PNA index (Fig. 2e). As the dipole structure shifted northeastward in the later period, the *ec1* of T_{2m} and Φ500 were highly related to the EPO index, where r ~ 0.78 of EPO and $ec1_{T2m}$ and r ~ 0.85 of EPO and $ec1_{\Phi500}$, while the correlations with the PNA index became insignificant.

Teleconnection patterns are widely documented to have huge impacts on the ice cover of the Great Lakes [Assel and Rodionov, 1998; Assel et al., 2000; Bai et al., 2012, 2015]. Table 1 examines the correlations between AMIC and climate indices averaged in December-February in the periods before and after the breakpoint. It is clear that AMIC in the earlier period was under the influences of ENSO, NAO, and PNA with significant correlation coefficients r = -0.65, -0.55, and -0.48, respectively, indicating the combination effects from multiple patterns [Bai et al., 2012; Wang et al., 2018]. It is worth noting that none of the well-known indices listed in Table 1 was correlated with AMIC in the later period, after the 1997/98 breakpoint. In the later period, the EPO index showed a significant negative correlation with AMIC. The EPO corresponds to a dipole pattern with the higher geopotential height anomaly located at the Gulf of Alaska and lower south of the eastern tropical Pacific during a negative EPO, and vice versa during positive phase. The negative correlation between EPO and AMIC indicates the importance of Φ500 over the Gulf of Alaska, which was consistent with the SVD results in the later period. Higher Φ500 over the Gulf of Alaska likely allowed the polar jet to loop into North America after crossing the Rocky Mountains, again the ridge-trough system, and steered the cold air mass from the Arctic into mid-latitude regions including the Great Lakes. As a result, the negative EPO likely generated a weather condition that is favorable to high AMIC.

	ENSO	PDO	NAO	AO	PNA	EPO
AMIC (1980-1997)	**-0.65**	0.03	**-0.55**	-0.35	**-0.48**	-0.38
AMIC (1998-2017)	0.02	0.26	0.08	0.18	-0.09	**-0.57**

Table 1 Correlation coefficient between AMIC and monthly climate indices averaged within DJF in the earlier (1980-1997) and later (1998-2017) periods. Numbers in bold indicate the 95% confidence interval.

How did sea ice loss over the Bering and Chukchi Seas in early winter, as represented by SIC_{ND}, contribute to the shift of the dipole pattern? Regressed Φ500 in December-February onto the preceding SIC_{ND} presented a clear connection between Φ500 and SIC_{ND} in the later period, after the 1997/98 breakpoint (Fig. 3). In the earlier period, the regression map of Φ500 revealed two positive centers over the east of the Bering and Chukchi Seas, the Gulf of Alaska, and the Arctic Archipelago (Fig. 3a). Most of the significant regions were located at the northern positive center close to CAA and there was no significant correlation over the Bering and Chukchi Seas.

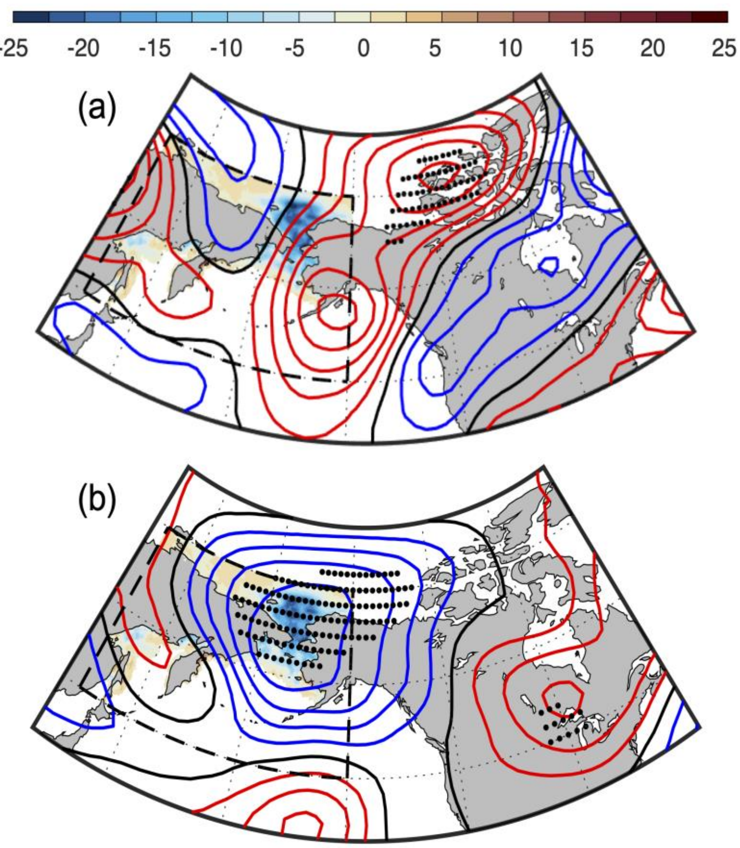

Figure 3. Regression maps of Φ500 averaged in Dec-Feb to sea ice concentration in Nov-Dec (SIC_{ND}, which is shown as a blue line in Fig.1a, of the (a) earlier (1980-1997) and the (b) later (1998-2017) periods. Difference of sea ice concentration between the two periods (later minus earlier period) in Nov-Dec is shown as color shading (same as in Fig. 1c).

The regression map of Φ500m in the later period showed a dipole pattern where the negative was centered over the Bering and Chukchi Seas and the positive was located in the Great Lakes and Northeast America (Fig. 3b). This dipole was similar but opposite to the SVD results in the later period (Fig. 2c). The significant regressions were concentrated over the Chukchi Sea and the Great Lakes. The negative regressions between SIC_{ND} and Φ500 in December-February were consistent with the correlation between SIC and AMIC (Fig. 1d) and the SVD results (Fig. 2c). This negative regression above the Bering-Chukchi Seas indicates that the lower (higher) SIC_{ND} contributed to forming the higher (lower) Φ500 anomaly in the following winter season, looping (blocking) the polar jet over the northwestern North America, steering (preventing) the cold Arctic air into mid-latitude, and eventually resulting in higher (lower) AMIC of the Great Lakes.

We further calculated the correlation between the AMIC and the monthly Φ500 and T_{2m} from November to February to understand the developments of AMIC-related atmospheric patterns in both periods (Fig. 4). In the earlier period, the dipole structure of AMIC-related Φ500 had its positive anomaly in the eastern North Pacific and the negative in North America from December to February (not in November), as seen in Fig. 4a. From these monthly correlation maps, the dipole of geopotential height seemed to develop from the subtropical region in December and then connected with the polar height in December. This dipole reached its minimum in February and formed a PNA-like pattern across the North Pacific and North America. The significant correlations with AMIC were located at the dipole center. The significant negative correlations between AMIC and T_{2m} was mainly located at the southwest portion of the negative geopolitical height over North America, indicating the forcing from the dipole structure of Φ500.

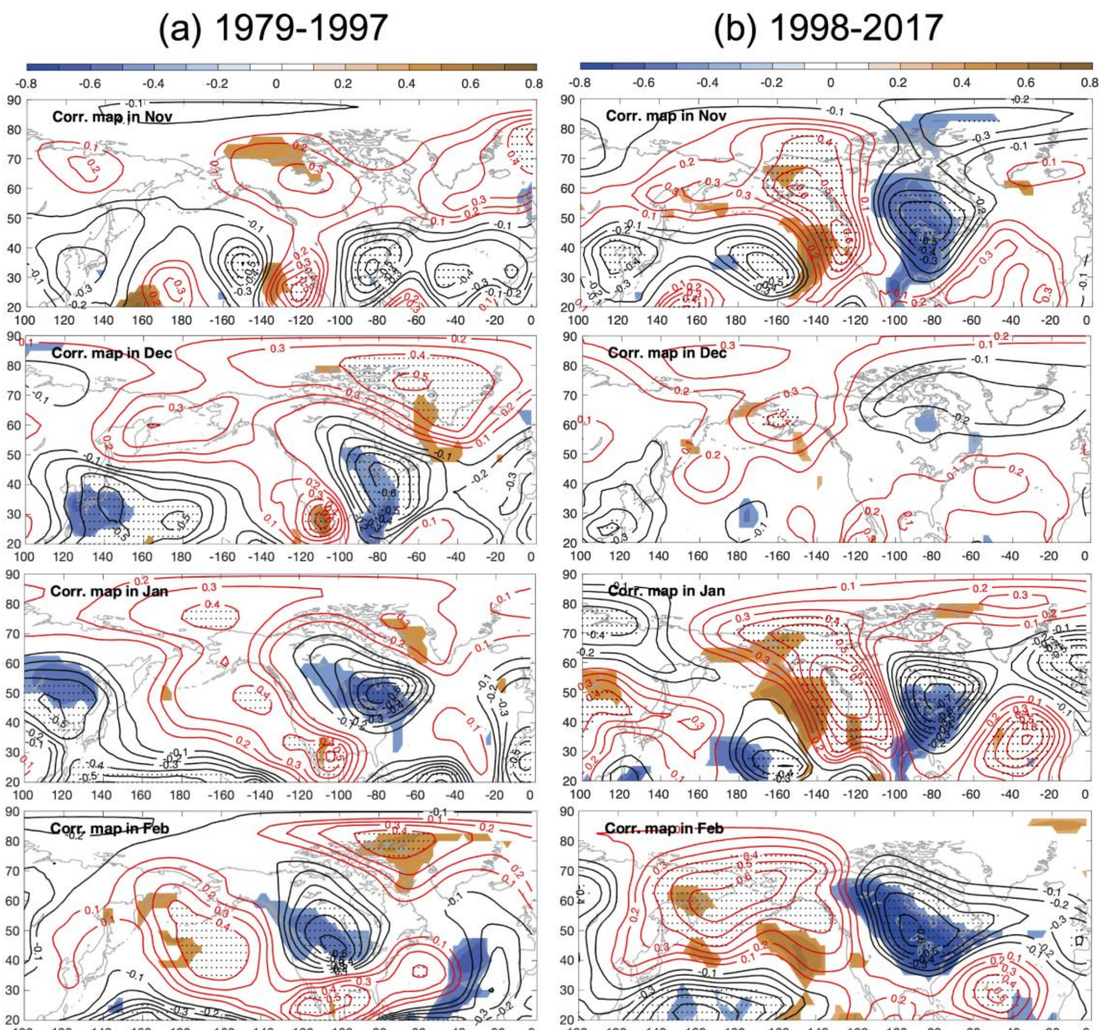

Figure 4. Monthly correlation maps between T_{2m} (color) and Φ500 (contour) with AMIC in (a) 1980 to 1997 (left) and (b) 1998 to 2017 (right). Red (black) contours indicate positive

(negative) correlation. Contour interval is every 0.1. Color regions and dots indicate the correlations reached 95% confidence interval.

The monthly correlation maps between the AMIC and Φ500 in the later period showed that the AMIC-related dipole structure was strengthened and appeared as early as November (Fig. 4b). The dipole structure, which was tied to AMIC, widely covered the eastern North Pacific and North America in November and the peak correlation was higher than any month in the earlier period. This strengthened dipole led to earlier cooling on the surface air temperature. The lowest negative correlation between the AMIC and the T_{2m} reached -0.74 over the Great Lakes. The wide range of this negative correlation also indicated an earlier cooling covering central North America in November. It is unclear why there was no distinct pattern in December related to the AMIC. Possible inferences could be the due to the recent warming and the delay of winter that eased the weather of December. The correlation maps in January and February both showed higher magnitudes in the dipole structure of Φ500 than the earlier period over the North Pacific and North America. The dipole structure shifted northward in February and the positive portion covered the entire Bering-Chukchi Seas. Evidently, the shifted, enhanced dipole structure provided a conduit for the cold air mass from the Arctic by steepening the North America ridge-trough system [Bai and Wang, 2012], which resulted in the strong negative correlation between AMIC and the surface air temperature. The dipole pattern might potentially contribute to the severe winter in recent years in which the eastern US experienced relative low temperature anomalies [Overland and Wang, 2018].

The cold anomaly over North America, due to the dipole structure of Φ500, was accompanied by the warm anomaly over the Alaska Peninsula. The positive portion of the dipole structure drove the warm air from the subtropical Pacific towards the north in November and January, prior to the high AMIC. This resulted in the contrast of surface air temperature between North America and the Alaska Peninsula, a potential indicator for predicting ice cover of the Great Lakes.

4 Summary and Discussion

A significant breakpoint in the winter of 1997/1998, which coincided with one of the largest ENSO events, was identified in this study. After the breakpoint, a predominant teleconnection pattern over North American and Western Alaska shifted and consequently AMIC and SIC_{ND} started to covary. Before the breakpoint, the AMIC had significant connections with ENSO, NAO, and PNA, indicating the combination effects from multiple climate indices. After the breakpoint, none of these well-known climate indices presented significant correlation with AMIC. Instead, the Eastern Pacific Oscillation (EPO) index solely presented significant negative correlation with AMIC. After this breakpoint, sea ice coverage over the Bering and Chukchi Seas in November and December experienced negative correlation with AMIC. The SVD analysis showed that the variations of AMIC before and after 1997 are strongly dominated by the dipole structure of Φ500 that steered the cold air from the Arctic to the Great Lakes region. Regression analysis suggested that the sea ice loss in earlier winter likely triggered changes in planetary waves (or the polar jet), propagating into the shift and enhancement of the ridge-trough system over the Rocky mountains, providing a conduit for the cold air mass from the Arctic into the Great Lakes region, resulting in high ice coverage. Some key questions arose. For instance, how exactly can sea ice anomalies over the Bering and Chukchi Seas alter a Rossby wave train and contribute to the dipole structure? The findings from this study warrant further investigations to fully understand the dynamical and thermodynamical processes of the connection between the AMIC and the sea ice coverage in the Bering Sea, Chukchi Sea, and the rest of the Arctic Ocean.

Acknowledgments, Samples, and Data

The annual maximum ice cover of the Great Lakes (AMIC) is obtained from the NOAA Great Lakes Environmental Research Laboratory (https://www.glerl.noaa.gov/data/ice/#historical). The monthly gridded Arctic sea ice concentration can be accessed at the National Snow and Ice Data Center (https://nsidc.org/data/g10010). The atmospheric data can be accessed at NCEP Gridded Climate Datasets (https://psl.noaa.gov/data/gridded/data.ncep.reanalysis2.html). The climate indices can be accessed at NOAA Climate Prediction Center (https://www.cpc.ncep.noaa.gov/data/teledoc/telecontents.shtml) and ESRL/PSL GEFS Reforecast 2 (https://psl.noaa.gov/data/climateindices/list/). This research was carried out with support of the National Oceanic and Atmospheric Administration (NOAA) Great Lakes Environmental Research Laboratory (GLERL), awarded to the Cooperative Institute for Great Lakes Research (CIGLR) through the NOAA Cooperative Agreement with the University of Michigan (NA12OAR4320071). This is GLERL contribution XXXX and CIGLR contribution XXXX.

References

Assel, R. A. (1992). Notes and correspondence Great Lakes Winter-Weather 700-hPa PNA Teleconnections. *Monthly Weather Review*, 2156–2163.

Assel, R. A. (1998). The 1997 ENSO event and implication for North American Laurentian Great Lakes winter severity and ice cover. *Geophysical Research Letters*, *25*(7), 1031–1033.

Assel, R. A., Janowiak, J. E., Boyce, D., O'Connors, C., Quinn, F. H., & Norton, D. C. (2000). Laurentian Great Lakes ice and weather conditions for the 1998 El Niño winter. *Bulletin of the American Meteorological Society*, *81*(4), 703–717. https://doi.org/10.1175/1520-0477(2000)081<0703:LGLIAW>2.3.CO;2

Assel, R. A., Janowiak, J. E., Young, S., & Boyce, D. (1996). Winter 1994 weather and ice conditions for the Laurentian Great Lakes. *Bulletin of the American Meteorological Society*, *77*(1), 71–88. https://doi.org/10.1175/1520-0477(1996)077<0071:WWAICF>2.0.CO;2

Assel, R. A., & Robertson, D. M. (1995). Changes in winter air temperatures near Lake Michigan, 1851-1993, as determined from regional lake-ice records. *Limnology and Oceanography*, *40*(1), 165–176. https://doi.org/10.4319/lo.1995.40.1.0165

Assel, R. A., Snider, C. R., & Lawrence, R. (1985). Comparison of 1983 Great Lakes Winter Weather and Ice Conditions with Previous Years. *Monthly Weather Review*, *13*(3), 291–303.

Assel, R., Cronk, K., & Norton, D. (2003). Recent trends in Laurentian Great Lakes ice cover. *Climatic Change*, *57*(1–2), 185–204. https://doi.org/10.1023/A:1022140604052

Assel, R., & Rodionov, S. (1998). Atmospheric teleconnections for annual maximum ice cover on the Laurentian Great Lakes. *International Journal of Climatology*, *18*(4), 425–442. https://doi.org/10.1002/(sici)1097-0088(19980330)18:4<425::aid-joc258>3.3.co;2-h

Bai, X., & Wang, J. (2012). Atmospheric teleconnection patterns associated with severe and mild ice cover on the Great Lakes, 1963-2011. *Water Quality Research Journal of Canada*, *47*(3–4), 421–435. https://doi.org/10.2166/wqrjc.2012.009

Bai, X., Wang, J., Austin, J., Schwab, D. J., Assel, R., Clites, A., … Leshkevich, G. (2015). A record-breaking low ice cover over the Great Lakes during winter 2011/2012: combined effects of a strong positive NAO and La Niña. *Climate Dynamics*, *44*(5–6), 1187–1213. https://doi.org/10.1007/s00382-014-2225-2

Bai, X., Wang, J., Sellinger, C., Clites, A., & Assel, R. (2012). Interannual variability of Great Lakes ice cover and its relationship to NAO and ENSO. *Journal of Geophysical Research: Oceans*, *117*(3). https://doi.org/10.1029/2010JC006932

Bamston, A. G., Chelliah, M., & Goldenberg, S. B. (1997). Documentation of a highly enso-related sst region in the equatorial pacific: Research note. *Atmosphere - Ocean*, *35*(3), 367–383. https://doi.org/10.1080/07055900.1997.9649597

Barnston, A., & Livezey, R. E. (1987). Classification, Seasonality and Persistence of Low-Frequency Atmospheric Circulation Pattern. *Monthly Weather Review*, *115*, 1083–1126.

Carmack, E., & Melling, H. (2011). Cryosphere: Warmth from the deep. *Nature Geoscience*, *4*(1), 7–8. https://doi.org/10.1038/ngeo1044

Cohen, J., Pfeiffer, K., & Francis, J. A. (2018). Warm Arctic episodes linked with increased frequency of extreme winter weather in the United States. *Nature Communications*, *9*(1), 1–12. https://doi.org/10.1038/s41467-018-02992-9

Cohen, J., Screen, J. A., Furtado, J. C., Barlow, M., Whittleston, D., Coumou, D., … Jones, J. (2014). Recent Arctic amplification and extreme mid-latitude weather. *Nature Geoscience*, *7*(9), 627–637. https://doi.org/10.1038/ngeo2234

Francis, J. A., Chan, W., Leathers, D. J., Miller, J. R., & Veron, D. E. (2009). Winter Northern Hemisphere weather patterns remember summer Arctic sea-ice extent. *Geophysical Research Letters*, *36*(7), 1–5. https://doi.org/10.1029/2009GL037274

Gillett, N. P., Stone, D. A., Stott, P. A., Nozawa, T., Karpechko, A. Y., Hegerl, G. C., … Jones, P. D. (2008). Attribution of polar warming to human influence. *Nature Geoscience*, *1*(11), 750–754. https://doi.org/10.1038/ngeo338

Hanson, H. P., Hanson, C. S., & Yoo, B. H. (1992). Recent Great Lakes Ice Trends. *Bulletin of the American Meteorological Society*, *73*(5), 577–584. https://doi.org/10.1175/1520-0477(1992)073<0577:rglit>2.0.co;2

Honda, M., Inoue, J., & Yamane, S. (2009). Influence of low Arctic sea-ice minima on anomalously cold Eurasian winters. *Geophysical Research Letters*, *36*(8), 1–6. https://doi.org/10.1029/2008GL037079

Hurrell, J. W. (1995). Decadal trends in the North Atlantic oscillation: Regional temperatures and precipitation. *Science*, *269*(5224), 676–679. https://doi.org/10.1126/science.269.5224.676

Kanamitsu, M., Ebisuzaki, W., Woollen, J., Yang, S.-K., Hnilo, J. J., Fiorino, M., & Potter, G. L. (2002). NCEP-DOE AMIP-II Renalalysys (R-2). *Bulletin of the American Meteorological Society*, *83*(11), 1631–1643. https://doi.org/10.1175/BAMS-83-11

Magnuson, J. J., Robertson, D. M., Benson, B. J., Wynne, R. H., Livingstone, D. M., Arai, T., … Vuglinski, V. S. (2000). Historical trends in lake and river ice cover in the Northern Hemisphere. *Science*, *289*(5485), 1743–1746. https://doi.org/10.1126/science.289.5485.1743

Magnuson, John J., Bowser, C. J., Assel, R. A., DeStasio, B. T., Eaton, J. R., Fee, E. J., … Schindler, D. W. (1995). *Region 1—Laurentian Great Lakes and Precambrian Shield. Proc. Symp. Report: Regional Assessment of Freshwater Ecosystems and Climate Change in North America*.

Mantua, N. J., Hare, S. R., Zhang, Y., Wallace, J. M., & Francis, R. C. (1997). A Pacific Interdecadal Climate Oscillation with Impacts on Salmon Production. *Bulletin of the American Meteorological Society*, *78*(6), 1069–1079. https://doi.org/10.1175/1520-0477(1997)078<1069:APICOW>2.0.CO;2

Mo, K., & Livezey, R. E. (1986). Tropical-Extratropical Geopotential Height Teleconnections during the Northern Hemisphere Winter. *Monthly Weather Review*, *114*(12), 2488–2515.

Niimi, A. J. (1982). Economic and Environmental Issues of the Proposed Extension of the Winter Navigation Season and Improvements on the Great Lakes-St. Lawrence Seaway System. *Journal of Great Lakes Research*, *8*(3), 532–549. https://doi.org/10.1016/S0380-1330(82)71991-4

Ogi, M., Taguchi, B., Honda, M., Barber, D. G., & Rysgaard, S. (2015). Summer-to-winter sea-ice linkage between the Arctic ocean and the Okhotsk sea through atmospheric circulation. *Journal of Climate*, *28*(12), 4971–4979. https://doi.org/10.1175/JCLI-D-14-00297.1

Overland, J. E., & Wang, M. (2018). Arctic-midlatitude weather linkages in North America. *Polar Science*, *16*(January), 1–9. https://doi.org/10.1016/j.polar.2018.02.001

Rodionov, S., & Assel, R. (2000). Atmospheric teleconnection patterns and severity of winters in the Laurentian Great Lakes basin. *Atmosphere - Ocean*, *38*(4), 601–635. https://doi.org/10.1080/07055900.2000.9649661

Rodionov, S., & Assel, R. A. (2001). A New Look at the Pacific/North American Index. *Geophysical Research Letters*, *28*(8), 1519–1522.

Rodionov, S., & Assel, R. A. (2003). Winter severity in the Great Lakes region: A tale of two oscillations. *Climate Research*, *24*(1), 19–31. https://doi.org/10.3354/cr024019

Serreze, M. C., & Francis, J. A. (2006). The Arctic Amplification Debate. *Climatic Change*, *76*(3–4), 241–264. https://doi.org/10.1007/s10584-005-9017-y

Smith, J. B. (1991). The Potential Impacts of Climate Change on the Great Lakes. *Bulletin of the American Meteorological Society*, *72*(1), 21–28. https://doi.org/10.1177/0958305x9800900403

Thompson, D. W. J., & Wallace, J. M. (1998). The Arctic oscillation signature in the wintertime geopotential height and temperature fields. *Geophysical Research Letters*, *25*(9), 1297–1300. https://doi.org/10.1029/98GL00950

Titze, D. J., & Austin, J. A. (2014). Winter thermal structure of Lake Superior. *Limnology and Oceanography*, *59*(4), 1336–1348. https://doi.org/10.4319/lo.2014.59.4.1336

Van Cleave, K., Lenters, J. D., Wang, J., & Verhamme, E. M. (2014). A regime shift in Lake Superior ice cover, evaporation, and water temperature following the warm El Niño winter of 1997-98. *Limnology and Oceanography*, *59*(6), 1889–1898. https://doi.org/10.4319/lo.2014.59.6.1889

Vanderploeg, H. A., Bolsenga, S. J., Fahnenstiel, G. L., Liebig, J. R., & Gardner, W. S. (1992). Plankton ecology in an ice-covered bay of Lake Michigan: utilization of a winter phytoplankton bloom by reproducing copepods. *Hydrobiologia*, *243–244*(1), 175–183. https://doi.org/10.1007/BF00007033

Wallace, J. M., & Gutzler, D. S. (1981). Teleconnections in the Geopotential Height Field during the Northern Hemisphere Winter. *Monthly Weather Review*, *109*(4), 784–812.

Walsh, J. E., Chapman, W. L., & Fetterer, F. (2016). Gridded Monthly Sea Ice Extent and Concentration, 1850 Onwards, Version 1.1. https://doi.org/10.7265/N5833PZ5

Wang, J., Bai, X., Leshkevich, G., Colton, M., Clites, A., & Lofgren, B. (2010). Severe ice cover on great lakes during winter 2008-2009. *Eos*, *91*(5), 41–42. https://doi.org/10.1029/2010EO050001

Wang, Jia, Bai, X., Hu, H., Clites, A., Colton, M., & Lofgren, B. (2012). Temporal and spatial variability of Great Lakes ice cover, 1973-2010. *Journal of Climate*, *25*(4), 1318–1329. https://doi.org/10.1175/2011JCLI4066.1

Wang, Jia, Kessler, J., Bai, X., Clites, A., Lofgren, B., Assuncao, A., … Leshkevich, G. (2018). Decadal variability of Great Lakes ice cover in response to AMO and PDO, 1963-2017. *Journal of Climate*, *31*(18), 7249–7268. https://doi.org/10.1175/JCLI-D-17-0283.1

Wang, Jia, Kessler, J., Hang, F., Hu, H., Clites, A., & Chu, P. (2017). Great Lakes Ice Climatology Update of Winters 2012-2017 : Seasonal Cycle , Interannual Variability , Decadal Variability , and Trend for the period. In *NOAA Technical Memorandum GLERL-170*. Retrieved from https://www.glerl.noaa.gov/pubs/tech_reports/glerl-170/tm-170.pdf

Yang, T. Y., Kessler, J., Mason, L., Chu, P. Y., & Wang, J. (2020). A consistent Great Lakes ice cover digital data set for winters 1973–2019. *Scientific Data*, *7*(1), 1–12. https://doi.org/10.1038/s41597-020-00603-1

Figures

Figure 1. (a) Annual maximum ice cover (AMIC, %) from 1980 to 2017 (red line with black dots). Blue line with black dots indicates the sea ice concentration (SIC) averaged within November-December over Bering Seas (black-dashed box in Fig.1c). Black solid lines and gray dashed lines indicate the means and standard deviations of AMIC in earlier (1980-1997) and later (1998-2017) periods. Green line indicates the t-test p-value of the separation year for periods before and after. Dotted and dotted-dashed lines indicate the 95% and 90% confidence level, respectively. (b) Scatter plot of dates of AMIC versus AMIC from 1980 to 2017. Crosses indicate the mean and error bars are the standard deviation for dates of AMIC (horizontal) and AMIC (vertical) of earlier (gray) and later (black) periods. (c) Sea ice concentration difference between the two periods (later minus earlier period). Dots indicate that the difference between the two periods reaches the 95% confidence interval based on t-test. Black-dashed box indicates the region for the blue line in Fig. 1a. (d) Scatter plot of the normalized sea ice concentration and AMIC (shown in Fig. 1a) for the earlier period (black) and later period (red).

Figure 2. Spatial patterns of SVD modes 1 for T_{2m} (color) and Φ500 (contour) averaged over December to February of (a) 1980 to 2017, (b) 1980 to 1997, and (c) 1998 to 2017. Expansion coefficients of T_{2m} ($EC1_{T2m}$, black) and Φ500 ($EC1_{\Phi500}$, blue) of (d) 1980 to 2017, and (e) 1980 to 1997 (years before vertical dashed line) 1998 to 2017 (years after vertical dashed line). All expansion coefficients are normalized by their respective standard deviations. Vertical dashed line in (e) indicates the year of 1997 for separation. SCF is the square covariance fraction and r is the correlation coefficient between the two expansion coefficients. Red line in (d) is the AMIC, green line in (e) is the PNA_r, and orange line in (e) is the EPO_r, where the subscript "*r*" indicates the reversed index. Both AMIC and EPO are normalized by their standard deviations, except for PNA. Corr(*A*, *B*) denotes the correlation coefficient between *A* and *B*. All Corr(*A*, *B*) listed here reach the 95% confidence interval.

Figure 3. Regression maps of Φ500 averaged in Dec-Feb to sea ice concentration in Nov-Dec (SIC_{ND}, which is shown as a blue line in Fig.1a, of the (a) earlier (1980-1997) and the (b) later (1998-2017) periods. Difference of sea ice concentration between the two periods (later minus earlier period) in Nov-Dec is shown as color shading (same as in Fig. 1c).

Figure 4. Monthly correlation maps between T_{2m} (color) and Φ500 (contour) with AMIC in (a) 1980 to 1997 (left) and (b) 1998 to 2017 (right). Red (black) contours indicate positive (negative) correlation. Contour interval is every 0.1. Color regions and dots indicate the correlations reached 95% confidence interval.

Tables

Table 1 Correlation coefficient between AMIC and monthly climate indices averaged within DJF in the earlier (1980-1997) and later (1998-2017) periods. Numbers in bold indicate the 95% confidence interval.

	ENSO	PDO	NAO	AO	PNA	EPO
AMIC (1980-1997)	**-0.65**	0.03	**-0.55**	-0.35	**-0.48**	-0.38
AMIC (1998-2017)	0.02	0.26	0.08	0.18	-0.09	**-0.57**